Materials Science in Semiconductor Processing 137 (2022) 106198

Contents lists available at ScienceDirect

Materials Science in Semiconductor Processing

journal homepage: www.elsevier.com/locate/mssp

Design investigation on 100 μm-thickness thin silicon PERC solar cells with assistance of machine learning

Heng Zhu, Wensheng Yan *, Yiming Liu, Die Hu, Yiteng Tu, Zhengtao Huang, Xinyu Tan **

Hubei Provincial Engineering Technology Research Center for Microgrid, College of Electrical Engineering & New Energy, China Three Gorges University, 8 University Avenue, Yichang, 443002, PR China

ARTICLE INFO

Keywords:
Solar cells
Passivated emitter and rear cell (PERC)
Optical and electrical designs
Machine learning
Multilayer perceptron algorithm

ABSTRACT

Thin crystalline silicon passivated emitter and rear cell (PERC) solar cells are a very prospective technology for next-phase photovoltaic development due to the potential of high cost effectiveness. The reduction of silicon wafer thickness can significantly save the costs, but there is a loss of cell efficiency if cell design is not conducted. For the thinned 100 μm-thickness PERC solar cells without design, the efficiency loss is pronounced from commercial 180 μm-thickness. In this paper, we have designed and optimized $SiO_2/SiN_x/SiN_x/SiO_x$ thin films (here two SiN_x layers have different refractive index) on the front surface and SiN_x/SiO_x thin films on the back surface for the standard front single-sided textured PERC cells. Based on this, we further design and investigate the case of double-sided textured PERC solar cells. Compared with the reference cell, the present designs can lead to the short-circuit current density increase by 0.6 mA/cm^2 and the open-circuit voltage enhancement by 10 mV for the front textured case, which causes the efficiency gain of 0.7% from 21.6% to 22.3%. For the double-sided textured cells, the efficiency has an extra increase of 0.6% from 22.3% to 22.9%. Finally, we have constructed the efficiency prediction model by using the multilayer perceptron algorithm in machine learning. It is found from the SHAP values that a significant effect of the front SiN_x thickness is observed to predict the performance of the PERC cells.

1. Introduction

PERC (Passivated Emitter and Rear Cell) solar cells, as a kind of high efficiency cells, have become a popular photovoltaic market leader in recent years [1,2]. In 1989, Blakers et al. first introduced the concept of PERCs [3]. After many years of development, PERC solar cells use the technologies such as atomic layer deposition to back passivate the cells, improving the quality of the passivation and achieving a high open-circuit voltage. As is known, long wavelength sunlight is not be well utilized in conventional cells when it passes through the thinner silicon wafers. However, higher reflectivity from the backside of PERC solar cells can effectively and better utilize long wavelength light and improve the long wavelength absorption, resulting in higher short-circuit current density [4–7]. In recent years, the technology for the preparation of PERC solar cells is well developed and the production conditions are compatible with those of back-aluminum solar cells [8,9]. Nowadays, industrially produced crystalline silicon (c-Si) PERC solar cells are typically in the thickness of 170–180 μm and have an average cell efficiency of 22% at this stage, but there has been continued research into how to further improve cell efficiency for the PERC cells with standard thickness [10–12]. Different from the focus of traditional PERC cells, here we focus on the cell design and efficiency investigation of significantly thinned silicon PERC cells, which is because that the cost of silicon material makes up 55%–60% of the cell cost and around 40% of the module cost. It is clear that remarkably reducing the thickness of c-Si PERC cells can significantly save the cost. But, the cell thickness reduction also causes cell efficiency loss. Therefore, a rational design of the cell structure is required to address the efficiency loss of the thin c-Si PERC cells [13].

In this work, we propose a solution for thin PERC solar cells with a thickness of 100 μm in order to solve the efficiency loss problem. We firstly use the 100 μm-thickness PERC cell with standard structure as a reference and calculatedly obtain its short-circuit current density (J_{sc}) of 39.3 mA/cm^2, the open-circuit voltage (V_{oc}) of 668 mV, and the efficiency of 21.6%, respectively. Next, we have designed and investigated two types of 100 μm-thickness PERC solar cells: standard front single-

* Corresponding author. .
** Corresponding author. .
E-mail addresses: yanws@ctgu.edu.cn (W. Yan), tanxin@ctgu.edu.cn (X. Tan).

https://doi.org/10.1016/j.mssp.2021.106198
Received 22 May 2021; Received in revised form 15 August 2021; Accepted 10 September 2021
Available online 13 September 2021

sided textured PERC cells and double-sided textured PERC cells. Here, we adopt $SiO_x/SiN_x/SiN_x/SiO_2$ structure design (here two SiN_x layers have different refractive index) on the front surface to improve the light trapping ability at short wavelengths and to optimize J_{sc} value. Meanwhile, this front SiO_2 thin film is also used to increase V_{oc} value of the PERC solar cell. The structural design of SiN_x/SiO_x on the back surface is used to enhance the light absorption at long wavelengths. Compared with the reference cell, this designed cell structure contributes to 0.6 mA/cm^2 higher and the V_{oc} value is 10 mV higher, resulting in the efficiency of 22.3%. Furthermore, the efficiency of the double-sided textured PERC solar cells is improved to 22.9%, which causes an absolute efficiency gain of 1.3% compared with the reference cell. To verify the validity of the simulation method, a comparison between the experiment and simulations is conducted for a 180 μm-thickness PERC cell due to that the experimental data of 100 μm-thickness PERC cell is rare at present. It is found that an overall excellent agreement is achieved. At last, we use machine learning to construct the multilayer perceptron (MLP) algorithm on the pycharm platform using the Scikit-learn module which is superior in handling highly correlated data, and then investigate the efficiency prediction model using the data obtained from the simulations. It is found that the effect of the front two SiN_x thin film thicknesses on the cell efficiency is the most important to the performance of the present solar cells.

2. Cell, model and simulations

2.1. Process of PERC solar cells

As shown in Fig. 1 (a), it is a cross-sectional schematic of a thin, p-type c-Si PERC solar cell with a cell thickness of 100 μm as a reference cell. In this cell, the front surface is a layer of SiN_x thin film with a thickness of 80 nm on the surface of textured Si, and its refractive index is 1.99. The diffusion method and laser doping are used to achieve lightly doped n^+ emitter and highly localized doped n^{++} emitter, namely, selective emitter (SE), respectively. At the rear side of PERC solar cell, there is a layer of Al_2O_3 thin film with the thickness of 6 nm and SiN_x with a thickness of 110 nm, where the refractive index of rear SiN_x is the same as that of the front surface. At the rear side, localized back surface field (LBSF) is also included. The cross-sectional schematic of the 100 μm-thick PERC solar cell with optical and electrical designs is shown in Fig. 1 (b). For the structure design of the front surface, a layer of SiO_2 film is deposited near the silicon substrate. The thickness of the front SiO_2 film is based on optical and electrical considerations. The SiO_2 film will not cause light absorption loss in the absorber, which can greatly improve the quality of the front end passivation and increase V_{oc} of the PERC solar cells. The main function of the front three-layer $SiO_x/SiN_x/SiN_x$ film is to enhance the absorption of short-wavelength light, where two SiN_x layers have different refractive indices for improved light antireflection loss. For the rear design, SiN_x/SiO_x film is selected to deal with light absorption loss at long wavelengths. This kind of film with graded refractive index distribution also achieves the purpose of reducing light reflectivity. Fig. 1(c) is for the double-sided textured cell, where an additional rear texture is conducted on the basis of Fig. 1 (b). All cell structures calculated in this work have all aluminium (Al) electrodes on the back. The electrical and optical properties of the back surface structure are evaluated. The effect of different cell surface structures on electrical performance of the thinned PERC solar cell is simulated by software Quokka 2 [14], getting the J_{sc}, V_{oc}, fill factor (FF) and cell efficiency of the thin PERC solar cells.

The present cell designs are valid for the PERC solar cells from the point of cell fabrication as shown in Fig. 2. The reference cell can be fabricated in the following experimental procedure: (1) The industrial technology for manufacturing solar cells begin with the texturing of the Si surface [15]. Standard damage etching and wet-chemical alkaline texturing like Cz wafers are used to achieve the random pyramid texture with a lower reflectance. The chemical treatment is used to reveal

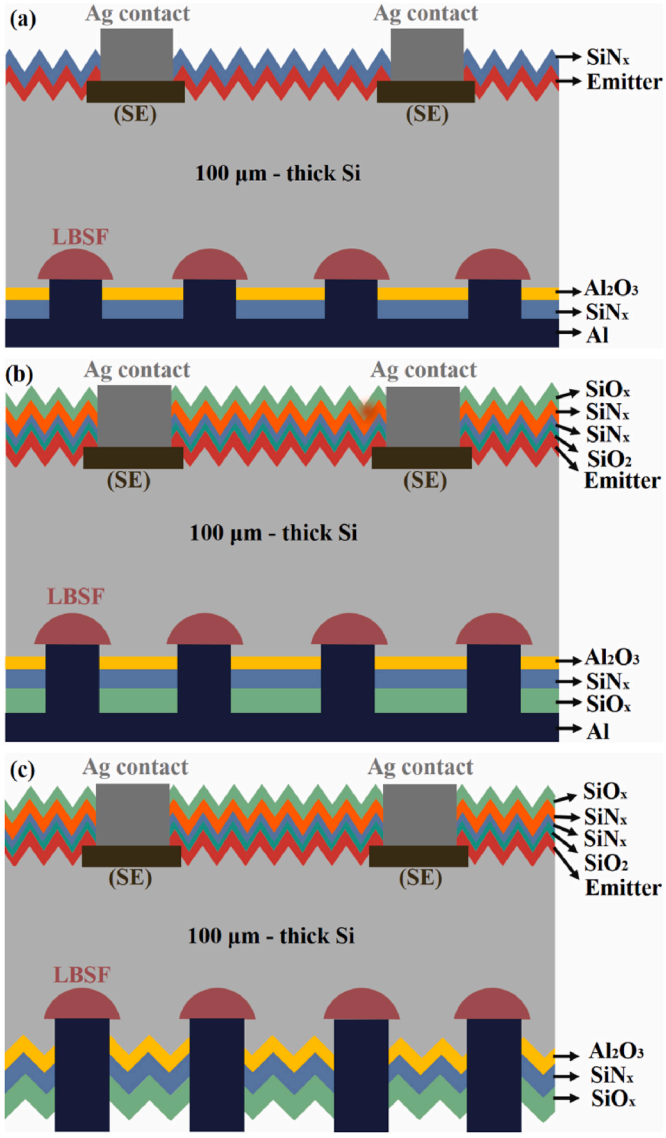

Fig. 1. (a) 100 μm-thick PERC solar cell with conventional structure as a reference; (b) front-sided textured 100 μm-thick PERC solar cell; (c) double-sided textured 100 μm-thick PERC solar cell.

pyramid structures with angle of 54.7° and depth of 3 μm. (2) Diffusion using $POCl_3$ as a precursor gas to form the n + emitter. The front selective emitter (SE) [16] is conducted under the front contacts by using local laser doping. (3) After diffusion, the phosphor silicate glass (PSG) and the protective coating behind it are removed simultaneously by HF (hydrofluoric acid) etching. (4) Thermal oxidation method is used to form a SiO_2 layer. (5) The passivation of the back side is guaranteed by the rapid atomic layer deposition (ALD) thin aluminum oxide (Al_2O_3) [17] layer. (6) SiN_x passivation layer deposited at the rear and SiN_x anti-reflective coating (ARC) layer deposited at the front by plasma enhanced chemical vapour deposition (PECVD) [18]. (7) Laser ablation of the line pattern to create localised contact, screen printing and co-fire techniques to ensure front and rear side metallization.

The EQE refers to the ratio of the number of photogenerated carriers successfully collected by the electrodes of the solar cell to the total number of incident photons. The quantum efficiency tester used in the experiment is composed of xenon light source, monochromator, filter, signal detector, test software and computer, etc. It can measure the quantum efficiency at wavelengths of 300–1200 nm. Stable monochromatic light is irradiated on the surface of the solar cell, and the cell

Fig. 2. Process flowchart of PERC solar cell fabrication.

is biased by a broadband bias light source. Finally, the signal is collected and the data is analyzed and displayed through the test software.

Ultraviolet–visible–near-infrared spectrophotometer can characterize reflectance. The reflectance test system consists of five main parts: light source, monochromator, sample cell, detector and recording device. The integrating sphere is the core of the reflectance test. Its main function is to eliminate the unevenness of the emitted light beam through multiple diffuse reflections of the incident light on the integrating sphere. Using the integrating sphere, the consistency of the final result can be reproduced, and the reliability of the final data is greatly improved. When combined with a spectrometer, the integrating sphere connects the output light to the entrance of the spectrometer to obtain the reflectance and wavelength relationship.

The conversion efficiency of solar cells is the key parameter to characterize the performance of solar cells which directly reflects the merits of solar cell performance. Optical atmospheric quality AM 1.5 g, irradiance of 1000 W/m^2 and a test temperature of 25 °C are used as standard test conditions to calibrate the performance parameters of solar cells. The J-V characteristic parameter measurement of solar cells enables direct measurement of electrical parameter values such as short-circuit current J_{sc}, open-circuit voltage V_{oc}, fill factor FF and conversion efficiency η.

2.2. Multilayer perceptron neural network

Machine learning is becoming a trend to assist the investigation of solar cells. It is possible to apply machine learning algorithms to the rapid prediction and screening of new designs of silicon solar cells. In particular, in manufacturing environments with large amounts of real solar cell data in the future, machine learning can identify the most appropriate process conditions to optimize yield, performance and cost of solar cell manufacturing. Multilayer Perceptron (MLP) [19,20], also known as Artificial Neural Network (ANN), in addition to the input and output layers, there can be multiple hidden layers in the middle. The simplest MLP has only one hidden layer, namely three-layer structure. A multilayer perceptron is fully connected between layers. The bottom layer of the multilayer perceptron is the input layer, the middle is the hidden layer, and the last is the output layer. The output term of this layer is the predicted value of the response variable. The MLP algorithm is superior in handling highly correlated data. ANN has generalization capabilities as it can process unseen data faster, use very few measurement data sets and is easier than other classical methods. So we have built the MLP algorithm using Scikit-learn module on pycharm platform, and then we construct the Efficiency Prediction Model (EPM) with the data obtained from the Quokka2 simulations.

The Root Mean Square Error (RMSE) is the most commonly used evaluation metric in machine learning, which measures the deviation between the observed and true values and characterizes prediction ability (efficiency) of the created model. In the learning process, the error is estimated by RMSE, defined as

$$RMSE = \sqrt{\frac{\sum_{i=1}^{N}(X_{Predicted} - X_{Actual})}{N}} \quad (1)$$

Where N is the number of data patterns in the independent dataset, $X_{Predicted}$ is the prediction, and X_{Actual} is the measured value of a data point.

Meanwhile, Pearson Correlation Coefficient (r) is widely used to assess the strength of linear correlation between two variables, and we use it to test the performance of the model.

$$r = \frac{n\sum x_i y_i - \sum x_i \sum y_i}{\sqrt{n\sum x_i^2 - (\sum x_i)^2}\sqrt{n\sum y_i^2 - (\sum y_i)^2}} \quad (2)$$

where n is the number of data patterns in the independent dataset; x_i is the i-th experimental value of x; y_i is the i-th predicted value of y.

3. Results and discussion

The absorption loss of light from 100 μm-thickness PERC solar cells is calculated and evaluated for thin crystalline silicon PERC solar cells by using the commercial software Sunsolve [21]. In the present model, the front texture adopts randomly distributed upright pyramids with the height of 3 μm and the angle of 54.7° which can be realized in the experiments. The solar spectrum adopts standard sunlight AM 1.5G and the incident light is vertical on the surface of solar cells. During the present simulations, the wavelength range is from 300 nm to 1200 nm with an interval of 20 nm. The parameter settings for the simulations are shown in Table 1.

For the reference cell, the light absorption curve is calculated by using the commercial software Sunsolve. At the same time, we carry out optimization calculations to determine the optimum thickness of each film to design a 100 μm-thick PERC cell, as shown in Fig. 1(b). Not only is the light absorption increased at short wavelengths, but also is the loss of light absorption addressed in the long wavelength range. The SiN_x and

Table 1
The main parameter settings for Sunsolve simulation.

Simulations	Descriptions	Parameters settings
Solar cells	Wafer	100 μm; 156.75μm × 156.75 μm
	Textures	Front side: Inverted spherical caps(Random, 54.7°, 3 μm high) Rear side: Inverted spherical caps(Random, 54.7°, 3 μm high)
	Antireflection coatings	Front side: 60 nm SiO_x(PEVCD); 20 nm SiN_x(PEVCD 1.91); 30 nm SiN_x(PEVCD 1.99); 10 nm SiO_2 Rear side:6 nm Al_2O_3(ALD on Si); 60 nm SiN_x(PEVCD 1.99); 110 nm SiO_x(PEVCD)

SiO_x films on the rear surface are found to be 60 nm and 110 nm, respectively, and the front $SiO_x/SiN_x/SiN_x$ thicknesses on the front surface are 60, 20 and 30 nm, respectively, as a result of optimization. Fig. 3 shows a graph of light absorption and reflection curves via the simulations. In the short wavelength range from 300 nm to 480 nm, it is found that the PERC solar cells with the present designed cell show a significant increase in light absorption compared to the reference cell, which is mainly due to the front $SiO_x/SiN_x/SiN_x$ structure design (refer to the resource file of Database Table 1 in the Support Information). The refractive indices of the two SiN_x on the front surface are 1.91 and 1.99, respectively. Such film design with a graded refractive index distribution can achieve a reduction in light reflectivity. Also, for the SiO_2 film on the front surface, the simulation results show that a thickness of 10 nm is the optimum thickness from an optical and electrical point of view. Higher V_{oc} is obtained from an outstanding passivation effect of SiO_2 thin film [22]. Furthermore, a significant reduction in light absorption loss can be seen in the long wavelength range from 900 to 1200 nm. This is mainly due to the SiO_x/SiN_x structural design at the rear surface.

It is known that when the photons are incident on the surface of a photosensitive device, some of the photons excite the photosensitive material to produce electron-hole pairs, forming an electric current. The ratio of the collected electrons (through processes such as internal electron-hole recombination) to the number of all incident photons is called the external quantum efficiency (EQE) [23]. To further investigate the enhancement of the J_{sc}, the EQE calculation results and comparison between the reference cell and designed cell are shown in Fig. 4, which includes reflections. During the present calculations, it is assumed

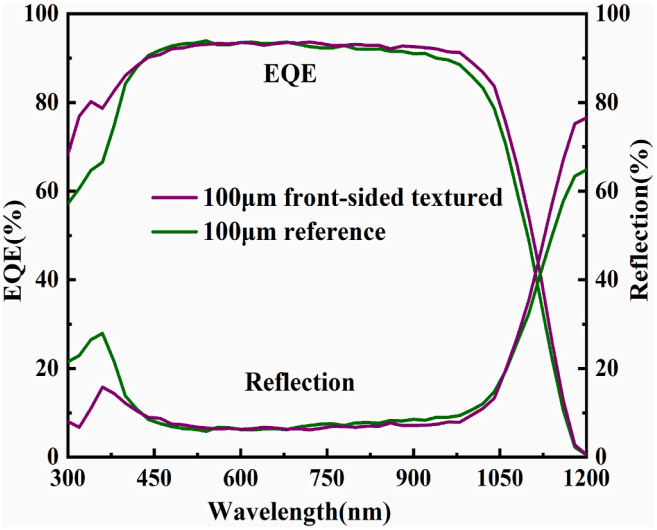

Fig. 4. The EQE and reflectance of the reference cell and the designed front textured PERC cell.

that the absorbed electron-hole pairs are all extracted (The resource file has been added to Database Table 2 in the Support Information section). It can be seen in Fig. 4 that the EQE shows a significant increase at short wavelengths from 300 to 420 nm compared to the reference cell, as well as a slight increase in frontal reflectance at longer wavelengths from 800 to 1150 nm. Compared to the reference cell, the front reflectance of the designed cell presents a significant decrease at the short wavelengths from 300 to 420 nm.

Light capture has a fundamental impact on the ability to generate photocurrent which heavily depends on the structure of the front and rear surfaces of the solar cell. In industry, the front surface typically adopts random upright pyramids to absorb the light, so the structure of the rear surface will be the object of investigation. The double-sided textured PERC solar cell is shown in Fig. 1(c), where the random pyramids have an angle of 54.7° and an average height of 3 μm. In Fig. 5, we compare the light absorption and reflection curves of a front-sided textured PERC cell and a double-sided textured PERC cell (The resource file has been added to Database Table 3 in the Support Information section). Since the reflection is primarily determined by the

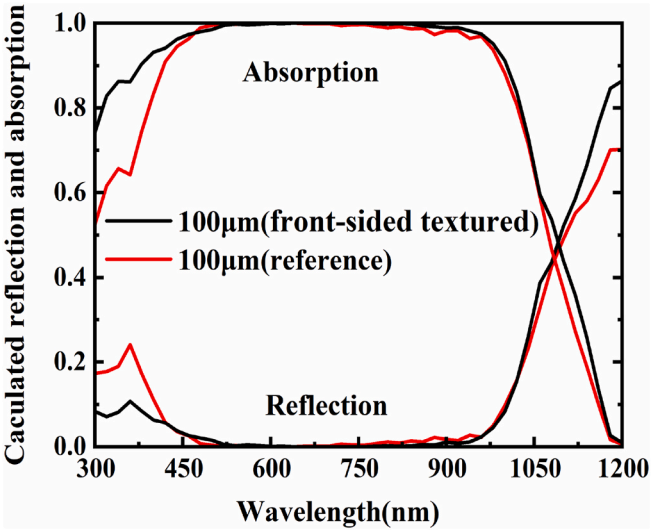

Fig. 3. Calculated front reflectance and cell absorption of 100 μm-thickness PERC solar cell (front-sided textured) and 100 μm-thickness PERC cell (reference) in the wavelength range from 300 to 1200 nm.

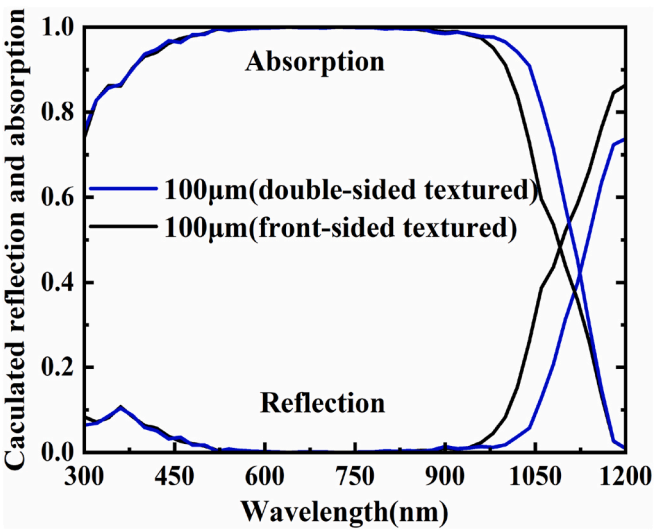

Fig. 5. Calculated front reflectance and cell absorption of 100 μm-thick PERC cell (front-sided textured) and 100 μm-thick PERC cell (double-sided textured) in the wavelength range from 300 to 1200 nm.

structure of the front surface and the anti-reflection coating, their characteristics are the same in the short wavelength range. In the wavelength range of 950–1150 nm, the effect of the rear surface texture becomes apparent. A significant increase in light absorption and decrease in the reflection curve can be clearly seen for the double-sided textured PERC solar cells. This indicates that there is a significant reduction in the reflection of photons in the long wavelength range at the rear surface of the cell, which captures more photons and allows for a boost in cell performance. Through the present design, the double-sided textured PERC solar cell can theoretically increase the photocurrent density by 0.99 mA/cm^2.

The PERC solar cells are simulated by Quokka 2 software to solve the carrier transport problem in quasi-neutral approximation silicon devices. The approach simplifies the general semiconductor carrier transport model by introducing conducting boundaries and quasi-neutral conditions. The conductivity boundary conditions omit the solution of the general set of semiconductor equations, including one transport equation for the minority and majority carriers and Poisson's equation for the electric potential. The charge carrier transport model described by the three coupled differential equations can be simplified so that it is solved by a set of only two differential equations. These simplifications have been well proven and cause no apparent loss of versatility or accuracy for silicon-based solar cell devices. The PERC unit cell is simulated by Quokka 2 software. Table 2 lists the initial parameters of the PERC cell, where these parameters are cited from reference. As a result, the efficiency of the PERC solar cells can be obtained.

The J-V responses are simulated for reference cell, front-sided textured cell, and double-sided textured cell. The results are listed in Table 3. The simulated J-V curves of the three types of PERC solar cells are shown in Fig. 6. It is seen in Table 3 that the reference PERC cell has an efficiency of 21.6%, while the designed single-sided textured PERC solar cell has an efficiency of 22.3%, which means a 0.7% increase in efficiency compared to the reference cell. This efficiency gain is from the improvements of both the V_{oc} and J_{sc}, where 10 mV-V_{oc} improvement is due to the adoption of the front SiO_2 surface, improving the passivation quality of the front surface, and the front $SiO_x/SiN_x/SiN_x$ structure contribute to J_{sc} improvement of 0.6 mA/cm^2. As shown in Table 3, the double-sided textured PERC solar cell has an efficiency of 22.9%, which has a 0.6% enhancement compared to the case of the designed cell with front-sided texture alone. This gain is attributed to the J_{sc} increase of by 0.5 mA/cm^2, mainly due to the additional light absorption enhancement in longer wavelength range from the rear surface texture.

Table 2
The input parameters for the present calculations on the designed PERC solar cells.

Region	Quokka2 Parameters	Value
Main	cell thickness	100 μm
	Front width	1000 μm
	Rear width	500 μm
	cell depth	200 μm
Front (Emitter)	Contact shape	Line
	Half width	19 μm
Emitter 1	Shape	Full area
	Sheet resistance	60Ω/□[a]
	Junction depth	0.5 μm[b]
	J_0 non-contacted	25fA/cm^2[b]
	J_0 contacted	57fA/cm^2[b]
	Contact resistivity	0.1 mΩ cm^2[b]
	Collection efficiency	1
Emitter 2	Shape	Line
	Sheet resistance	60Ω/□[a]
	Junction depth	0.5 μm[b]
	J_0 non-contacted	150fA/cm^2[b]
	J_0 contacted	400fA/cm^2[a]
	Contact resistivity	0.1 mΩ cm^2[b]
	Collection efficiency	0.9[a]
Bulk	Resistivity	1.5 mΩ cm[a]
	Background lifetime	750μs
BSF	Contact shape	Line
	Half width	19 μm
	Sheet resistance	60 Ω/□[a]
	Junction depth	0.5 μm[b]
	J_0 non-contacted	100 fA/cm^2[b]
	J_0 contacted	250 fA/cm^2[a]
	Contact resistivity	1 mΩ cm^2[b]

[a] Cite the value of reference [24].
[b] Cite the value of reference [25].

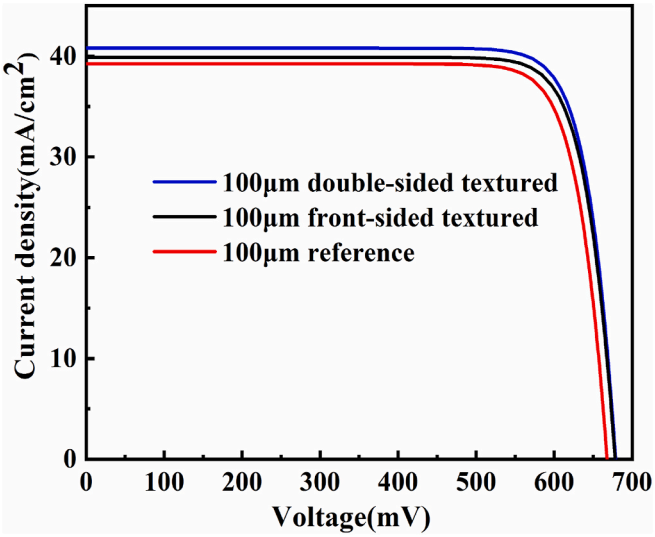

Fig. 6. Simulated J-V curves of the three PERC solar cells.

In order to improve and verify the validity of the present simulations, we have conducted the simulations to reproduce an experimental report on 180 μm-thickness PERC solar cells (Refer to this literature [26]), where the experimentally measured average efficiency of the cells are 21.94%, and our simulation results by using the Quokka2 simulations gives an efficiency of 21.9%, (The initial parameters for the simulations has been added to Database Table 4 in the Support Information section), where the detailed results are listed in Table 4. It contains the experimental results and the software simulation results in the literature, as well as our simulation results. The slight deviation in the open-circuit voltage is due to some experimental uncertainty, but the rest of the data are in general agreement. This comparison shows that the present design and simulation results can offer a valuable guidance on future experiments for thinned silicon solar cells towards high efficiency at low cost.

The MLP algorithm is applied to the present cell model investigations. Because the present improvement is from additional thin film design and optimization at front and rear surface, we use MLP algorithm to investigate the ranking of these thin films according to the importance to the efficiency gain. So the input X is the five thicknesses of SiN_x and SiO_x on the front and rear surfaces of the PERC solar cell, corresponding to Fig. 1(a). X_1 is the thickness of SiO_x on the front surface, X_2 is the thickness of SiN_x on the first layer of the front surface, X_3 is the thickness of SiN_x on the second layer of the front surface, X_4 is the thickness of SiN_x on the back surface, X_5 is the SiO_x thickness on the rear surface, and the output Y is the efficiency of the PERC solar cell. Efficiency prediction model is built to determine how the thickness of each layer affects the efficiency of the cell. From the data obtained from

Table 3
The simulated PV parameters of the three cells.

Cell type	J_{sc} (mA/cm^2)	V_{oc} (mV)	FF	η
Reference	39.3	668	82.2%	21.6%
Designed front texture	39.9	678	82.4%	22.3%
Designed double texture	40.8	679	82.6%	22.9%

Table 4
The measured (Exp.) and simulated (Sim.) PV parameters of PERC cells.

Cell type	J_{sc} (mA/cm^2)	V_{oc} (mV)	FF	η
Exp:180 μm-thick PERC cell	40.46	672.10	80.68%	21.94%
Sim:180 μm-thick PERC cell (In the literature)	40.61	671.50	80.30%	21.90%
Sim:180 μm-thick PERC cell (Our Simulation)	40.60	669.00	80.60%	21.90%

Quokka 2 simulations, we obtain a database and divide it into training dataset, validation dataset, and test datasets. Here there are 139 training data sets and 17 test data sets, respectively.

A simple prediction of the cell efficiency was carried out using the MLP algorithm. A mean square error of 0.0484 and a coefficient of R of 0.984 were obtained, which can be seen to exhibit a strong correlation. The prediction of the efficiency by the MLP algorithm is shown in Fig. 7. It is seen that there is a high linear fit between the tested and predicted values, indicating an excellent result is achieved. The predicted values obtained by the efficiency prediction model (EPM) are very close to the 17 simulated values in the test set. This indicates the superiority of the MLP algorithm. It shows that the MLP algorithm can predict well the efficiency of the PERC solar cell.

The SHAP values [27,28] can visualize the importance of feature values and the positive and negative correlation effects on the final results. As shown in Fig. 8, we choose the MLP algorithm model and then use SHAP to interpret the EPM. The SHAP shows how the 5 variables (inputs) contribute to the efficiency of the PERC solar cell (outputs). The density scatter plot shows all the data and the order of the features is in descending order of the average absolute value of SHAP, which is the most important feature of the model. The wide area indicates that a large number of samples were collected. The color on the right side indicates the feature value, red indicates high feature value, blue indicates low feature value, and the horizontal axis indicates positive or negative SHAP value. As can be seen from Fig. 8, among the five elements, the main effect on the solar efficiency is X_2 and X_3 (e.g. the thicknesses of the first and second layer of SiN_x on the front surface). With the increasing thickness of SiN_x on the front surface, there will be a significant decrease in the efficiency of PERC solar cells.

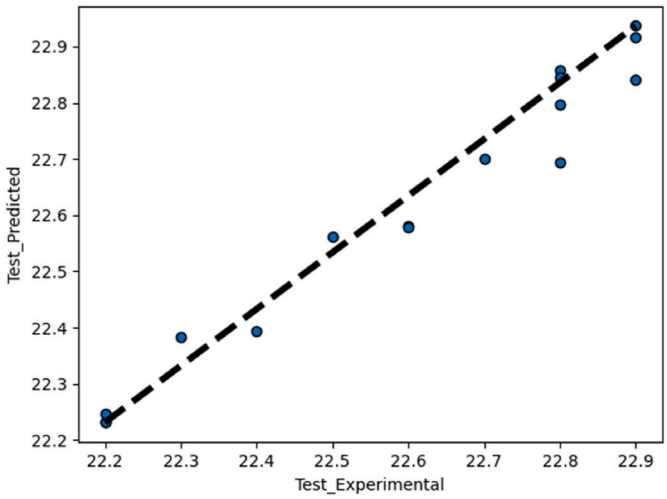

Fig. 7. The cell efficiency is predicted by the MLP algorithm and the results show the correlation between the data and the predicted results.

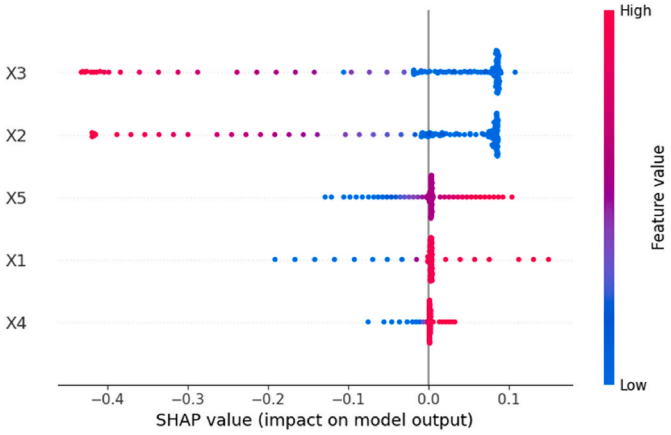

Fig. 8. Thickness importance ranking of PERC solar cells obtained from SHAP value.

4. Conclusion

The remarkable reduction in thickness of crystalline silicon PERC solar cells can significantly save the cost, but a loss of cell efficiency is suffered. For the 100 μm-thickness thin PERC solar cells without design, the efficiency loss is even more pronounced. For this purpose, the optical and electrical designs were carried out to address the efficiency loss of the 100 μm-thickness cell. When a front design of $SiO_2/SiN_x/SiN_x/SiO_x$ is used on the front surface of the PERC solar cell along with a SiN_x/SiO_x design on the rear surface, the J_{sc} is elevated by 0.6 mA/cm^2 compared to the reference cell. Also, the efficiency is increased from 21.6% to 22.3% with an absolute gain of 0.7%. The V_{oc} is increased by 10 mV, which is mainly attributed to the SiO_2 film used on the front surface that improves the passivation quality. We also investigated and designed a double-sided textured PERC solar cell with the efficiency of 22.9% and J_{sc} of 40.8 mA/cm^2. The MLP algorithm is used to investigate and identify the effect of these adopted layers on the efficiency and the correlation between the data and the predicted results.

CRediT authorship contribution statement

Heng Zhu: Conceptualization, Data curation, Formal analysis, Investigation, Methodology, Software, Visualization, Writing – original draft. **Wensheng Yan:** Conceptualization, Methodology, Software, Writing – review & editing, Resources, Investigation, Validation. **Yiming Liu:** Software, Resources, Investigation, Validation. **Die Hu:** Resources, Investigation, Supervision, Writing – review & editing. **Yiteng Tu:** Formal analysis. **Zhengtao Huang:** Software, Formal analysis. **Xinyu Tan:** Supervision, Resources, Writing – review & editing.

Declaration of competing interest

The authors declare that they have no known competing financial interests or personal relationships that could have appeared to influence the work reported in this paper.

Acknowledgements

This work was supported by National Natural Science Foundation of China (Grant No. U1765105, 52007104) and 111 Project (D20015) of China.

Appendix A. Supplementary data

Supplementary data to this article can be found online at https://doi.org/10.1016/j.mssp.2021.106198.

References

[1] R. Brendel, S. Steckemetz, K. Bothe, Fine-Line printed 5 busbar PERC solar cells with conversion efficiencies beyond 21%, in: 29th European Photovoltaic Solar Energy Confer-Ence and Exhibition, 2014, pp. 621–626, https://doi.org/10.4229/EUPVSEC20142014-2DO.3.4.

[2] N. Balaji, D. Lai, V. Shanmugam, Pathways for efficiency improvements of industrial PERC silicon solar cells, Sol. Energy 214 (2021) 101–109, https://doi.org/10.1016/j.solener.2020.11.025.

[3] A.W. Blakers, A. Wang, A.M. Milne, 22.8 percent efficient silicon solar cell, Appl. Phys. Lett. 55 (1989) 1363–1365, https://doi.org/10.1063/1.101596.

[4] Z.R. Du, N. Palina, J. Chen, Impact of KOH etching on laser damage removal and con-tact formation for Al local back surface field silicon wafer solar cells, in: 27th European Photovoltaic Solar Energy Conference and Exhibition, 2012, pp. 1230–1233, https://doi.org/10.4229/27thEUPVSEC2012-2AV.6.13.

[5] T. Roder, P. Grabitz, S. Eisele, 0.4% Absolute efficiency gain of industrial solar cells by laser doped selective emitter, in: Photovoltaic Specialists Conference (PVSC), 2009 34th IEEE, 2009, pp. 871–873, https://doi.org/10.1109/PVSC.2009.5411149.

[6] Z. Du, N. Palina, C. Jia, Rear-Side contact opening by laser ablation for industrial Screen-Printed aluminium local back surface field silicon wafer solar cells, Energy Procedia 25 (2012) 19–27, https://doi.org/10.1016/j.egypro.2012.07.003.

[7] H. Huang, J. Lv, Y. Bao, Data of ALD Al_2O_3 rear surface passivation, Al_2O_3 PERC cell performance, and cell efficiency loss mechanisms of Al_2O_3 PERC cell, Data in Brief 11 (C) (2017) 19–26, https://doi.org/10.1016/j.dib.2016.12.030.

[8] Y. Lv, Y.F. Zhuang, W.J. Wang, Towards high-efficiency industrial p-type mono-like Si PERC solar cells, Sol. Energy Mater. Sol. Cells 204 (2020) 110202, https://doi.org/10.1016/j.solmat.2019.110202.

[9] R. Eicke Weber, Energy research at the Fraunhofer Institute for solar energy systems, Energy Technol. 2 (1) (2014), https://doi.org/10.1002/ente.201305021, 3-3.

[10] P. Saint-Cast, S. Werner, J.G. Greulich, Analysis of the losses of industrial-type PERC solar cells, Phys. Status Solidi 214 (3) (2016) 1600708, https://doi.org/10.1002/pssa.201600708, 1-1600708.7.

[11] M. Matthias, F. Gred, B. Bernd, Loss analysis of 22% efficient industrial PERC solar ce-lls, Energy Procedia 124 (2017) 131–137, https://doi.org/10.1016/j.egypro.2017.09.322.

[12] B. Min, A roadmap toward 24% efficient PERC solar cells in industrial mass production, IEEE J. Photovolt. (2017) 1541–1550, https://doi.org/10.1109/JPHOTOV.2017.2749007.

[13] W.S. Yan, X.Y. Tan, L. Guan, Solution of efficiency loss in thinned silicon PERC solar cells, Renew. Energy (2021) 165, https://doi.org/10.1016/j.renene.2020.10.134.

[14] A. Fell, A free and fast Three-Dimensional/Two-Dimensional solar cell simulator featuring conductive boundary and Quasi-Neutrality approximations, IEEE Trans. Electron. Dev. 60 (2) (2013) 733–738, https://doi.org/10.1109/TED.2012.2231415.

[15] K. Fabianand, B. Till, B. Miriam, Influence of solder pads to PERC solar cells for module integration, Energy Procedia 38 (2013) 368–374, https://doi.org/10.1016/j.egypro.2013.07.291.

[16] S.J. Eisele, T.C. Roeder, J.R. Koehler, 18.9% efficient full area laser doped silicon solar cell, Appl. Phys. Lett. 95 (13) (2009) 133501, https://doi.org/10.1063/1.3232208, 133501-3.

[17] J. Schmidt, B. Veith, R. Brendel, Effective surface passivation of crystalline silicon using ultrathin Al_2O_3 films and Al_2O_3/SiN_x stacks, Phys. Status Solidi RRL 3 (9) (2009) 287–289, https://doi.org/10.1002/pssr.200903272.

[18] T. Dullweber, J. Schmidt, Industrial silicon solar cells applying the passivated emitter and rear cell (PERC) Concept-A review, IEEE J. Photovolt. 6 (5) (2016) 1366–1381, https://doi.org/10.1109/JPHOTOV.2016.2571627.

[19] A.H. Elsheikh, S.W. Sharshir, M. Abd Elaziz, Modeling of solar energy systems using artificial neural network: a comprehensive review, Sol. Energy 180 (2019) 622–639, https://doi.org/10.1016/j.solener.2019.01.037.

[20] B. Cortés, R.T. Sánchez, J.J. Flores, Characterization of a polycrystalline photovoltaic cellusing artificial neural networks, Sol. Energy 196 (2020) 157–167, https://doi.org/10.1016/j.solener.2019.12.012.

[21] https://www.pvlighthouse.com.au/sunsolve.

[22] F. Gervais, Handbook of Optical Constants of Solids Ii, 1985, https://doi.org/10.1080/716099804a. Boston Academic Press.

[23] F. Koppens, T. Mueller, P. Avouris, Photodetectors based on graphene, other two-dimensional materials and hybrid systems, Nat. Nanotechnol. 9 (10) (2014) 780–793, https://doi.org/10.1038/nnano.2014.215.

[24] F. Andreas, P.P. Altermatt, A detailed Full-Cell model of a 2018 commercial PERC solar cell in Quokka 3, IEEE J. Photovolt. 8 (2018) 1443–1448, https://doi.org/10.1109/JPHOTOV.2018.2863548, 8.

[25] A. Fell, K.R. Mcintosh, P.P. Altermatt, Input parameters for the simulation of silicon solar cells in 2014, IEEE J. Photovolt. 5 (4) (2017) 1250, https://doi.org/10.1109/JPHOTOV.2015.2430016.

[26] P. Wang, Numerical study of mono-crystalline silicon solar cells with passivated emitter and rear contact configuration for the efficiency beyond 24% based on mass production technology, J. Semiconduct. 41 (6) (2020) 85–91.

[27] S. Lundberg, S.I. Lee, A unified approach to interpreting model predictions, NIPS (News Physiol. Sci.) (2017) 4768–4777.

[28] S. Behara, T. Poonawala, T. Thomas, Crystal structure classification in ABO_3 perovskites via machine learning, Comput. Mater. Sci. (2020) 110191, https://doi.org/10.1016/j.commatsci.2020.110191.